Received: *April 16, 2000,* Accepted: *May 11, 2000*

Numerical analysis of fractional charge solutions on the torus

Álvaro Montero

Center for Theoretical Physics, Laboratory for Nuclear Science and Department of Physics, Massachusetts Institute of Technology Cambridge, Massachusetts 02139, USA

E-mail: montero@mitlns.mit.edu

Abstract: We study by numerical methods a particular kind of SU(N) Yang-Mills solutions of the euclidean equations of motion which appear on the torus when twisted boundary conditions are imposed. These are instanton-like configurations with the peculiarity of having fractional topological charge. We focus on those solutions with minimal non-trivial action $S = 8\pi^2/\mathrm{N}$ and extract their properties in a few different cases, paying special attention to the $N \to \infty$ limit.

Keywords: Non-perturbative Effects, Solitons Monopoles and Instantons, Lattice Gauge Field Theories.

JHEP05(2000)022

Contents

1. Introduction **1**

2. Numerical minimization of the action **4**

3. The solutions **5**
3.1 Gauge-invariant quantities 6
3.1.1 Global quantities 6
3.1.2 Energy profile 8
3.1.3 Action density 8
3.1.4 Eigenvalues of $\mathbf{F}_{\mu\nu}$ 10
3.1.5 Colour orientation of the field strength 13
3.1.6 Polyakov loops and structure of vacuum 14
3.2 Gauge-dependent quantities 16
3.2.1 Eigenvalues of $\mathbf{A}_i$ 16
3.2.2 Colour orientation of the potential 18
3.2.3 Twist matrix $\mathbf{\Omega_4}$ 18

4. Conclusions **19**

A. Analytic solutions **21**
A.1 't Hooft construction 21
A.2 Some examples 22
A.3 Changing the gauge 23

1. Introduction

Quite some time ago 't Hooft [1] pointed out some very special features which arise while formulating gauge theories on a torus (a review can be found in ref. [2]). They are related to the freedom in choosing boundary conditions for the gauge potential: since only local, gauge invariant quantities are required to be periodic, periodicity of the gauge potential has to be satisfied only up to a gauge transformation. Under displacement of the gauge potential by a torus period l_ν in direction $\hat{\nu}$

$$\mathbf{A}_\mu(x + l_\nu\hat{\nu}) = \mathbf{\Omega}_\nu(x)\mathbf{A}_\mu(x)\mathbf{\Omega}^\dagger_\nu(x) - \imath\mathbf{\Omega}_\nu(x)\partial_\mu\mathbf{\Omega}^\dagger_\nu(x)\,, \quad \mu = 1, \ldots, 4\,, \tag{1.1}$$

with $\mathbf{\Omega}_\nu(x_{\mu\neq\nu})$ SU(N) matrices, also known as the twist matrices. The choice of such matrices is arbitrary up to a consistency condition derived from the requirement of single-valuedness of the gauge potential. Built in two ways from $\mathbf{A}_\mu(x_\nu, x_\rho)$ (through $\mathbf{A}_\mu(x_\nu + l_\nu, x_\rho)$ and $\mathbf{A}_\mu(x_\nu, x_\rho + l_\rho)$) single-valuedness for $\mathbf{A}_\mu(x_\nu + l_\nu, x_\rho + l_\rho)$ implies

$$\mathbf{\Omega}_\mu(x_\nu + l_\nu)\mathbf{\Omega}_\nu(x_\mu) = \mathbf{\Omega}_\nu(x_\mu + l_\mu)\mathbf{\Omega}_\mu(x_\nu)\mathrm{Exp}\left(-\frac{\imath 2\pi n_{\mu\nu}}{\mathrm{N}}\right) \tag{1.2}$$

with $n_{\mu\nu}$ a gauge invariant antisymmetric tensor of integers, defined modulo N and independent of x (this twist factor is allowed due to the invariance of $\mathbf{A}_\mu$ under a gauge transformation with an element of the center $\mathbb{Z}_\mathrm{N}$ of SU(N)). Indeed, the actual choice of the twist matrices is irrelevant and only the consistency conditions given by $n_{\mu\nu}$ matter. Whenever $n_{\mu\nu} \neq 0$ (mod$N$), for some μ, ν, we say the boundary conditions are twisted. The twist is reflected in a gauge invariant way through the non-trivial periodicity of the Polyakov loops, defined on the torus as

$$\begin{aligned}\mathcal{L}_\mu(x) &= \frac{1}{\mathrm{N}}\,\mathrm{Tr}\,(\mathbf{L}_\mu) = \\ &= \frac{1}{\mathrm{N}}\,\mathrm{Tr}\left(\mathrm{Texp}\left\{\imath\int_{\gamma_{\mu(x,x')}} \mathbf{A}_\nu dx^\nu\right\}\mathbf{\Omega}_\mu(x')\mathrm{Texp}\left\{\imath\int_{\gamma_{\mu(x',x)}} \mathbf{A}_\nu dx^\nu\right\}\right)\end{aligned} \tag{1.3}$$

with $\gamma_{\mu(a,b)}$ a straight line in the positive μ direction starting at a and ending at b and x' the border of the torus patch. Periodicity holds only up to the twist factors, i.e.

$$\mathcal{L}_\mu(x + l_\nu\hat{\nu}) = \mathrm{Exp}\Big(-\frac{\imath 2\pi n_{\mu\nu}}{\mathrm{N}}\Big)\mathcal{L}_\mu(x)\,. \tag{1.4}$$

With twisted boundary conditions the topological charge Q is no longer necessarily an integer:

$$Q = \frac{1}{16\pi^2}\int \mathrm{Tr}\left(\mathbf{F}_{\mu\nu}\tilde{\mathbf{F}}_{\mu\nu}\right)d_4x = \nu - \frac{\kappa}{\mathrm{N}} \quad \text{with } \nu, \kappa \in \mathbb{Z}\,, \tag{1.5}$$

κ is associated to the matrix of integers $(n_{\mu\nu})$ through

$$\kappa = \frac{1}{4}n_{\mu\nu}\tilde{n}_{\mu\nu} = \vec{k}\cdot\vec{m}\,, \tag{1.6}$$

with $k_i = n_{0i}$, $n_{ij} = \epsilon_{ijk}m_k$. The mathematical proof of this relation for the topological charge can be found in [3]. Then Q is fractional and proportional to 1/N whenever $\vec{k}\cdot\vec{m} \neq 0$ modulo N (non-orthogonal twist). This implies, through Schwarz-inequality, that the action of any configuration is bounded from below by

$$S = \frac{1}{2}\int \mathrm{Tr}\left(\mathbf{F}_{\mu\nu}\mathbf{F}_{\mu\nu}\right)d_4x \geq 8\pi^2|Q| = 8\pi^2\left|\nu - \frac{\kappa}{\mathrm{N}}\right| \tag{1.7}$$

with the bound saturated for self or anti-self dual configurations ($\mathbf{F}_{\mu\nu} = \pm\tilde{\mathbf{F}}_{\mu\nu}$).

It is clear that whenever $\kappa \neq 0$ (modulo N) there is an obstruction for zero-action configurations. Minimal action is attained in such cases if $|\nu - \kappa/\mathrm{N}| = 1/\mathrm{N}$ with $S = 8\pi^2/\mathrm{N}$. These are in fact the kind of solutions we will describe in this paper.

Some of these fractional charge solutions have already been found either analytically or numerically. 't Hooft has explicitly constructed non-abelian solutions with constant field strength which turn out to be (anti-)self-dual whenever the sides of the torus satisfy certain relations (see [4] for details or appendix A at the end of this paper). There are also a few numerical studies of solutions with non-constant field strength. The first one is presented in ref. [5] and it is obtained there the fractional charge solution with $|Q| = 1/2$ and $S = 4\pi^2$ for the SU(2) group, on an $L^3 \times T$ torus with $T \gg L$ and satisfying twisted boundary conditions given by the twist vectors $\vec{m} = (1, 1, 1)$ and $\vec{k} = (1, 1, 1)$. A full parametrization of the field strength $\mathbf{F}_{\mu\nu}$, and of the gauge field $\mathbf{A}_\mu$ for this solution is presented in ref. [6]. Another SU(2) solution is presented in [7], in this case the fractional charge solution with $|Q| = 1/2$ and $S = 4\pi^2$, on a torus $L^2 \times T^2$ with $T \gg L$ and satisfying the appropriate boundary conditions to have the properties of a vortex. The same kind of solution for the SU(3) group, with $|Q| = 1/3$ and $S = 8\pi^2/3$, is presented in ref. [8], and the generalization to SU(N) group with $N > 3$ can be found in [9]. In this article we present a numerical study of SU(N) solutions, with charge $|Q| = 1/N$ and action $S = 8\pi^2/N$, and living on an $L^3 \times T$ torus with $T \gg L$. Some preliminary results have been presented in [10].

These configurations are interesting by itself from a mathematical point of view, and physically interesting for their possible relevance in low energy phenomena like the confinement property or the breaking of the chiral symmetry. As has been pointed out in [4] these solutions may play a role in the properties of the theory in the limit of large number of colors, N. One of the arguments to question the contribution of instantons to long-distance phenomena as confinement is based on the large-N expansion [11]. Any instanton mediated interaction is suppressed by the semi-classical factor $\exp(-8\pi^2/g^2)$, since the large-N limit is achieved while keeping $g^2\mathrm{N}$ fixed, integer charge instantons are (at least in the dilute gas picture) naively suppressed by $\exp(-N)$. The argument no longer holds for twisted instantons with action $8\pi^2/N$. Another interesting point is the possible relation between the center vortex picture of confinement, proposed in [12] and now being investigated [13]–[17], and fractional charge solutions. As have been pointed out in [7, 8, 9], it is possible to built vortex configurations in R^4 from solutions of the Yang-Mills equations of motion in T^4. We also want to mention the model of confinement based in fractional charge objects presented in ref. [18], and some favourable results shown in [19].

The paper is structured as follows. In section 2 the numerical method to obtain the solutions is briefly described. We will be interested in solutions living on an $L^3 \times T$ torus with $T \gg L$ which, in the limit $T \to \infty$, represent vacuum to vacuum tunneling. The analysis will be restricted to spatial twist $\vec{m} = (1, 1, 1)$. Section 3 presents a detailed analysis of these solutions. Our conclusions are presented in section 4. Finally, we include appendix A with the analytic solutions obtained through 't Hooft construction. Their relation with the cases we have studied is discussed through the text.

2. Numerical minimization of the action

To generate numerically the minimal action configurations we follow the method which has allowed to successfully extract these kind of solutions for other sizes of the torus and values of the number of colors in refs. [5]–[10]. We use the standard discretization of Yang-Mills theories on the lattice [20]. We work on $N_s^3 \times N_t$ lattices, $N_t \gg N_s$, with variables defined on each link of the lattice taking values on $N \times N$ unitary matrices $\hat{\mathbf{U}}_\mu(n)$. The lattice action used is the Wilson action,

$$S_W = \sum_{n,\mu,\nu} \mathrm{Tr}\left(1 - \hat{\mathbf{U}}_\mu(n)\hat{\mathbf{U}}_\nu(n+\hat{\mu})\hat{\mathbf{U}}_\mu^\dagger(n+\hat{\nu})\hat{\mathbf{U}}_\nu^\dagger(n)\right), \tag{2.1}$$

where μ and ν specify directions (from 1 to 4) and $\hat{\mu}$, $\hat{\nu}$ are unit vectors along the corresponding direction, $n_\mu = 1, \ldots, N_\mu$.

The link variables $\hat{\mathbf{U}}_\mu(n)$ satisfy the (twisted) boundary conditions,

$$\hat{\mathbf{U}}_\mu(n + N_\nu\ \hat{\nu}) = \mathbf{\Omega}_\nu(n)\ \hat{\mathbf{U}}_\mu(n)\ \mathbf{\Omega}_\nu^\dagger(n+\hat{\mu}), \tag{2.2}$$

where $N_4 = N_t$, $N_i = N_s$, $i = 1,2,3$ and $\mathbf{\Omega}_\mu$ are the twist matrices with consistency condition,

$$\mathbf{\Omega}_\mu(n + N_\nu\hat{\nu})\ \mathbf{\Omega}_\nu(n) = \mathbf{\Omega}_\nu(n + N_\mu\hat{\mu})\ \mathbf{\Omega}_\mu(n)\ \mathrm{Exp}\left(\frac{-2\pi\imath n_{\mu\nu}}{\mathrm{N}}\right). \tag{2.3}$$

It is possible to make a change of variables

$$\mathbf{U}_\mu(N_\mu, n_\nu) = \hat{\mathbf{U}}_\mu(N_\mu, n_\nu)\mathbf{\Omega}_\mu(n_\nu), \qquad \mathbf{U}_\mu(n_\mu \neq N_\mu, n_\nu) = \hat{\mathbf{U}}_\mu(n_\mu \neq N_\mu, n_\nu) \tag{2.4}$$

such that the new link variables are strictly periodic. In terms of the new links

$$S_W = \sum_{n,\mu,\nu} \mathrm{Tr}\left(1 - Z^*_{\mu\nu}(n)\mathbf{U}_\mu(n)\mathbf{U}_\nu(n+\hat{\mu})\mathbf{U}_\mu^\dagger(n+\hat{\nu})\mathbf{U}_\nu^\dagger(n)\right), \tag{2.5}$$

where $Z_{\mu\nu}(n) \in \mathbb{Z}_\mathrm{N}$ take the values: $Z_{\mu\nu}(n) = 1$ for all plaquettes except the one at the top-right corner in the (μ,ν) plane which is equal to $\mathrm{Exp}(-2\pi i n_{\mu\nu}/\mathrm{N})$.

The strategy to obtain the solution is minimize the lattice action with respect to the variable $\mathbf{U}_\mu(n)$ (this minimization procedure is usually known as cooling). We use the Cabibbo-Marinari-Okawa algorithm [21] in which each link variable is updated in the way: $\mathbf{U}_\mu(n) \to \mathbf{A}\mathbf{U}_\mu(n)$, where $\mathbf{A}$ is an SU(N) matrix built from an SU(2) matrix $\mathbf{a}$ which is embedded into one of the $N(N-1)/2$ subgroups of SU(N). Once we obtain the matrix $\mathbf{a}$ minimizing the new action $S_W(\mathbf{A}\mathbf{U}_\mu(n))$, we update the link variable $\mathbf{U}_\mu(n)$, and repeat the procedure for all the $N(N-1)/2$ subgroups of SU(N) and for all lattice sites. This constitutes one cooling sweep. We iterate this procedure up to we obtain that the Wilson action is stable with a given precision (in this work, the eight relevant digit) and close to the value of the expected continuum action: $S = 8\pi^2/N$.

3. The solutions

As mentioned in the introduction, we are interested in solutions with minimal non-trivial action,

$$S = 8\pi^2|Q| = \frac{8\pi^2}{N}\,, \tag{3.1}$$

on a volume $[-L/2, L/2]^3 \times [-T/2, T/2]$, with $T \gg L$. When $T \to \infty$ these solutions represent vacuum to vacuum tunneling.

We have restricted our analysis to the following non-orthogonal twist tensors:

1. Spatial twist, always $\vec{m} = (1,1,1)$.

2. Temporal twist, two cases:

   - $\vec{k} = (1,0,0)$ for $N = 3,4,5,8,10$ the solution is in this case anti-self-dual, $Q = -1/N$.
   - $\vec{k} = (n,n,n)$ for $N = 3n+1 = 4,7,10,13,19,25$ the solution is here self-dual, $Q = 1/N$.

A list of all the lattices analyzed is presented in table 1.

From the lattice configurations we can easily derive information concerning continuum quantities. Part of it can be extracted in a gauge invariant way, such is the case for instance of the eigenvalues of the field strength or the Polyakov loops. However to derive information concerning the gauge potential gauge fixing is needed.

The continuum field strength tensor is extracted, up to $\mathcal{O}(a^2)$, from the clover average of the plaquette:

$$\mathbf{Q}_{\mu\nu}(n) = \frac{1}{4} \tag{3.2}$$

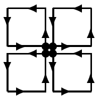

through

$$\mathbf{F}_{\mu\nu}(na) = \frac{1}{a^2}\frac{1}{2i}\left[\mathbf{Q}_{\mu\nu}(n) - \mathbf{Q}^\dagger_{\mu\nu}(n) - \frac{\mathbb{1}}{\mathrm{N}}\,\mathrm{Tr}\left(\mathbf{Q}_{\mu\nu}(n) - \mathbf{Q}^\dagger_{\mu\nu}(n)\right)\right]. \tag{3.3}$$

In terms of the gauge fixed links the gauge potential is,

$$\mathbf{A}_\mu\left[\left(n+\frac{1}{2}\right)a\right] = \frac{1}{a}\frac{1}{2i}\left[\mathbf{U}^{gf}_\mu(n) - \mathbf{U}^{gf\dagger}_\mu(n) - \frac{\mathbb{1}}{\mathrm{N}}\,\mathrm{Tr}\left(\mathbf{U}^{gf}_\mu(n) - \mathbf{U}^{gf\dagger}_\mu(n)\right)\right]. \tag{3.4}$$

The Polyakov loops $\mathbf{L}_\mu(x)$ are simply given on the lattice by the ordered product of the μ-links corresponding to the path $\gamma_\mu(x)$ in eq. (1.3).

Non-gauge invariant information about the configurations will be presented in the temporal gauge: $\mathbf{A}_4 = 0$. In addition we fix $\mathbf{A}_i(t = -\infty) = 0$ which is allowed because in the $T \to \infty$ limit fractional instantons describe vacuum-to-vacuum tunneling. In this gauge $\mathbf{A}_i(t = \infty) = -\imath \mathbf{\Omega}_4\, \partial_i\, \mathbf{\Omega}_4^\dagger$, with $\mathbf{\Omega}_4$ the temporal twist matrix, and the spatial twist matrices are constant. This is not yet a complete gauge fixing, we still have the freedom to make a global gauge transformation and also to multiply the twist matrices by an element of the center of the group. We have made use of the global gauge transformation to bring the spatial twist matrices to a particular form. An explicit construction of constant spatial twist matrices compatible with the twist $\vec{m} = (1, 1, 1)$ can be easily found, following 't Hooft [4]:

$$\mathbf{\Omega}_3 = \mathbf{Q}\,, \qquad \mathbf{\Omega}_2 = \mathbf{P}^{N-1}\,, \qquad \mathbf{\Omega}_1 = e^{i2\pi p/N}\mathbf{P}\mathbf{Q}^{N-1} \tag{3.5}$$

with p an integer number taking values $p = 1, 2, \ldots, \mathrm{N}$, and $\mathbf{P}$, $\mathbf{Q}$ the matrices,

$$\mathbf{P} = \begin{pmatrix} 0 & 1 & \cdots & 0 \\ \cdots & \cdots & \cdots & \cdots \\ 0 & 0 & \cdots & 1 \\ (-1)^{N+1} & 0 & \cdots & 0 \end{pmatrix}, \qquad \mathbf{Q} = e^{i\pi(1-N)/N} \begin{pmatrix} \phi_0 & 0 & \cdots & 0 \\ 0 & \phi_1 & \cdots & 0 \\ \cdots & \cdots & \cdots & \cdots \\ 0 & 0 & \cdots & \phi_{N-1} \end{pmatrix}, \tag{3.6}$$

where $\phi_n = \exp(i2\pi n/N)$ with $n = 0, 1, \ldots, \mathrm{N} - 1$.

The invariance under multiplication by an element of the center of the group is fixed by imposing that the Polyakov loops take the value $Ae^{i\pi}$ at the position where the energy density of the solution is maximal.

On the lattice the $\mathbf{A}_4 = 0$, $\mathbf{A}_i(t = -T/2) = 0$ gauge is implemented by transforming the corresponding link variables to the identity. The gauge transformation, $\omega(n)$, which implements the change, is constructed in the following way: choose a point in the time slice $t = -T/2$, i.e. $n^0 = (n_t = 1, \vec{n}^0)$; $\omega(n)$ is the product of the link variables along a certain path connecting n^0 with $n = (n_t, n_x, n_y, n_z)$. In particular we choose $n^0 = (1, 1, 1, 1)$ and the path such that it reaches the point n first in the x direction up to n_x, then in the y direction up to n_y, in the z direction up to n_z and finally in the t direction up to n_t. In this gauge the information about the twist matrices is encoded in the links $\mathbf{U}_0(n_t = N_t)$, $\mathbf{U}_i(n_t = 1, n_i = N_s)$, the latter are rotated to the form indicated in eq. (3.5) .

3.1 Gauge-invariant quantities

3.1.1 Global quantities

In table 1 we give the values obtained for the action S, electric and magnetic parts of the action, S_e and S_b respectively, and topological charge Q:

$$S = \frac{1}{2}\int \mathrm{Tr}\,(\mathbf{F}_{\mu\nu}\mathbf{F}_{\mu\nu})\, d_4x = \int \mathrm{Tr}\,\left(\mathbf{E}_i^2 + \mathbf{B}_i^2\right) d_4x\,,$$

$$S_e = \int \mathrm{Tr}\left(\mathbf{E}_i^2\right) d_4x\,, \qquad S_b = \int \mathrm{Tr}\left(\mathbf{B}_i^2\right) d_4x\,,$$
$$Q = \frac{1}{16\pi^2}\int \mathrm{Tr}\left(\mathbf{F}_{\mu\nu}\tilde{\mathbf{F}}_{\mu\nu}\right) d_4x = \frac{1}{4\pi^2}\int \mathrm{Tr}\left(\vec{\mathbf{E}}\vec{\mathbf{B}}\right) d_4x\,, \tag{3.7}$$

where $\mathbf{E}_i = \mathbf{F}_{4i}$ and $\frac{1}{2}\epsilon_{ijk}\mathbf{F}_{ij} = \mathbf{B}_k$. We can see from the data that the configurations obtained are (anti-)self-dual to a very good degree, being therefore solutions of the euclidean equations of motion. Those values are very near to the continuum expected values $S\mathrm{N}/8\pi^2 = 1$, $S_e\mathrm{N}/8\pi^2 = 0.5$, $S_b\mathrm{N}/8\pi^2 = 0.5$ and $Q\mathrm{N} = \pm 1$.

The first thing we should check is the scaling of the solutions. Without loss of generality we set the spatial length to $l_s = 1$, being then the lattice spacing $a = 1/N_s$. To see how the continuum limit $a \to 0$ is approached we vary the lattice spacing while keeping all other parameters fixed (among them the ratio N_t/N_s). We fit the N and a^2 dependence of the action to the expression $S\mathrm{N}/8\pi^2 = 1 - \Delta a^2/(\mathrm{N}\sqrt{\mathrm{N}})$ and obtain that for the value $\Delta = 8.893$ the data in table 1 are well described with errors smaller than the 0.2%. From this fit we understand how the continuum limit is approached for any value of N, and also that the N dependence is such that the

Sol.	Group	$\vec{k}$	Size	$S\mathrm{N}/8\pi^2$	Q N	$S_e\mathrm{N}/8\pi^2$	$S_b\mathrm{N}/8\pi^2$
	SU(3)	$(1,0,0)$	$6^3\times 18$	0.95409	-0.95370	0.47817	0.47592
	SU(3)	$(1,0,0)$	$7^3\times 21$	0.96623	-0.96602	0.48393	0.48230
	SU(3)	$(1,0,0)$	$8^3\times 24$	0.97413	-0.97401	0.48768	0.48645
I.1	SU(3)	$(1,0,0)$	$10^3\times 30$	0.98343	-0.98338	0.49210	0.49133
I.2	SU(4)	$(1,0,0)$	$8^3\times 32$	0.98273	-0.98267	0.49168	0.49105
I.3	SU(5)	$(1,0,0)$	$8^3\times 40$	0.98742	-0.98738	0.49387	0.49355
I.4	SU(8)	$(1,0,0)$	$5^3\times 40$	0.98377	-0.98368	0.49194	0.49183
I.5	SU(10)	$(1,0,0)$	$6^3\times 48$	0.99204	-0.99201	0.49465	0.49739
II.1	SU(4)	$(1,1,1)$	$8^3\times 32$	0.98275	0.98268	0.49166	0.49109
	SU(7)	$(2,2,2)$	$3^3\times 21$	0.94440	0.94346	0.47284	0.47155
	SU(7)	$(2,2,2)$	$5^3\times 35$	0.98020	0.98008	0.49026	0.48994
II.2	SU(7)	$(2,2,2)$	$8^3\times 56$	0.99229	0.99228	0.49613	0.49617
II.3	SU(10)	$(3,3,3)$	$4^3\times 40$	0.98192	0.98180	0.49100	0.49092
II.4	SU(13)	$(4,4,4)$	$4^3\times 52$	0.98801	0.98794	0.49399	0.49401
	SU(19)	$(6,6,6)$	$2^3\times 38$	0.97324	0.97200	0.48729	0.48594
II.5	SU(19)	$(6,6,6)$	$3^3\times 57$	0.98812	0.98804	0.49405	0.49406
II.6	SU(25)	$(8,8,8)$	$2^3\times 50$	0.98205	0.98187	0.49109	0.49096

Table 1: Set of studied solutions. All quantities are defined on eq. (3.7). In the first column we label the solutions for reference in other tables.

lattice corrections decrease with increasing N. This property will be discussed further later on, it implies that for large N we can obtain good continuum results already on rather coarse lattices, this is a rather general property which, as we will see, affects other quantities apart from the integrated action and charge densities.

3.1.2 Energy profile

The energy profile, defined as

$$\epsilon(t) = \int \mathrm{Tr}\left(E_i^2(\vec{x},t) + B_i^2(\vec{x},t)\right) d_3\vec{x}\,, \tag{3.8}$$

is located on a region of size $\sim N/3$ and has only one maximum for all values of N up to $N = 13$ (instanton profile) and a double peak structure for the values $N = 19, 25$. In figures 1a and 1b we show the scaling with the lattice spacing for the solutions with $N = 3$ and $N = 19$. We can see that points coming from lattices with different sizes describe very similar curves, scaling towards the same continuum function.

For values of N up to $N = 13$, $\epsilon(t)$ is well fitted by

$$\phi(t) = \frac{1}{A\cosh(wt) + Bt^2 + C}\,. \tag{3.9}$$

The values obtained for the parameters A, B, C, w are given in table 2. For the values $N = 19, 25$ we fit to the expression $(\phi(t - t_0) + \phi(t + t_0))/2$ and also in table 2 we give the results of these fits.

The N dependence is such that

$$\epsilon(t) \simeq \frac{\phi(t/\mathrm{N})}{\mathrm{N}^2} \tag{3.10}$$

as illustrated in figures 1c and 1d where $\mathrm{N}^2\epsilon(t)$ is plotted as a function of t/N for $\vec{k} = (1, 0, 0)$ and $\mathrm{N} = 4, 5, 8, 10$ in figure 1c and for $\vec{k} = (n, n, n)$ and $\mathrm{N} = 4, 7, 10, 13, 19, 25$ in figure 1d. We also plot in figure 1d the energy profile for the abelian solution described in appendix A (eqs. (A.14), (A.16) and (A.17)). We plot $N^2\epsilon(t) = 24\pi^2$ for the values of t/N between $t/N = -1/6$ and $t/N = 1/6$. This is the profile for the selfdual abelian solution in the $\mathrm{N} \to \infty$ limit. We can see that the energy profiles of the solutions with $\vec{k} = (n, n, n)$ are approaching the one of the abelian solution in the $\mathrm{N} \to \infty$ limit.

3.1.3 Action density

Defined as,

$$S(\vec{x},t) = \mathrm{Tr}\left(\mathbf{E}_i^2(\vec{x},t) + \mathbf{B}_i^2(\vec{x},t)\right). \tag{3.11}$$

For values of N up to $N = 13$, the action density has only one maximum what we will call the center of the instanton. We fit the center and their first nearest neighbors

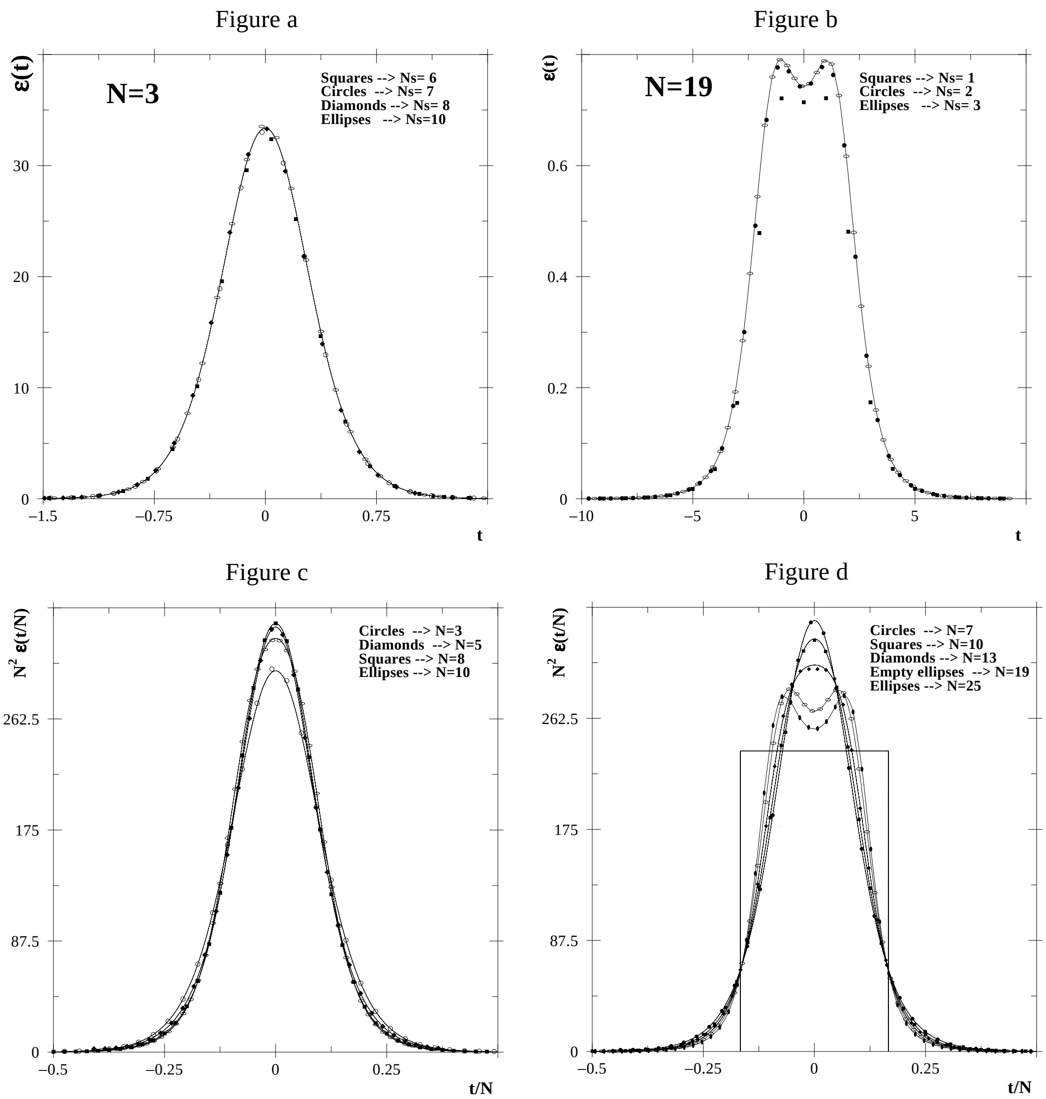

Figure 1: In figures a and b it is shown the energy profile as a function of time calculated with different lattice sizes for the solutions with $N = 3$ and $N = 19$, respectively. In figures c and d it is shown the N behavior of the energy profile, plotting N^2 times the value of the profile as a function of t/N, in figure c for solutions with $\vec{k} = (1, 0, 0)$ and in figure d with $\vec{k} = (n, n, n)$. The continuum curves are the fits to the function (3.9) given in table 2.

to the expression,

$$S(\vec{x}, t) = S_0 \left(1 - \sum_i \frac{(x_i - x_i^0)^2}{a_i^2} - \frac{(t - t^0)^2}{a_t^2} \right), \tag{3.12}$$

where S_0 is the height, x_i^0, t^0 the position and a_i, a_t the width of the maximum. The values obtained are shown in table 3. For the values $N = 19, 25$ we observe two maximum in the action density and we make the same fit for each one. The results are also shown in table 3. In both cases, the errors are obtained from the

Sol.	N	A	B	C	Nw	t_0	χ^2/N_t
I.1	3	0.00863	0.03009	0.02132	17.95	0.0	0.0001500
I.2	4	0.02371	−0.01394	0.02588	17.10	0.0	0.0000468
I.3	5	0.04700	−0.04251	0.02766	16.51	0.0	0.0000490
I.4	8	0.11399	−0.07989	0.07554	17.54	0.0	0.0000016
I.5	10	0.22671	−0.20144	0.08006	17.26	0.0	0.0000074
II.1	4	0.02357	−0.01222	0.02602	17.11	0.0	0.0000454
II.2	7	0.07820	−0.03956	0.06456	17.63	0.0	0.0000037
II.3	10	0.17808	−0.15184	0.12957	18.23	0.0	0.0000131
II.4	13	0.41834	−0.34723	0.13673	17.94	0.0	0.0000427
II.5	19	1.79852	−0.59304	−1.08299	18.93	1.24	0.0000542
II.6	25	2.02385	−0.59827	−0.82069	22.86	1.74	0.0000168

Table 2: Results of the fit to the energy profile.

difference between the same quantities calculated for the electric and magnetic part of the action. We can see that with increasing N all maximum become spatially flat. In fact, this is a general and important property of the solutions; when N is large some quantities, among them the action density, are spatially independent. In particular this implies that all the coordinate dependence of the action density comes through the time dependence of the energy profile $\epsilon(t)$ defined above. This fact allows to easily understand the decrease of the lattice artifacts with increasing N since generally constant fields give rise to a much smoother, continuum-like, behavior.

3.1.4 Eigenvalues of $\mathbf{F}_{\mu\nu}$

Since the solution is (anti) self-dual we only give the results for $\mathbf{B}_i$. The main properties for the eigenvalues of $\mathbf{F}_{\mu\nu}$ are illustrated in figures $2a$, $2b$, $2c$ and $2d$. We only show the results for the solutions with twist $\vec{k} = (n, n, n)$ because the same properties are obtained for the solutions with twist $\vec{k} = (1, 0, 0)$.

In figure $2a$ we show the eigenvalues of $\mathbf{B}_1$ for the solutions with $N = 7$ and $\vec{k} = (2, 2, 2)$. Very similar results are obtained if we plot $\mathbf{B}_2$ or $\mathbf{B}_3$ instead of $\mathbf{B}_1$. That we plot is the spatial average of each eigenvalue as a function of time. The error bars mean spatial dispersion of the eigenvalues (difference between the maximum and minimum value of the eigenvalue at each temporal point). The first property we observe is spatial independence of the eigenvalues. This property also holds for values of $N \geq 7$ as shown in figures $2b$, $2c$ and $2d$. From figure $2a$ we observe that we obtain good results from very coarse lattices. In this figure we plot points coming from lattices with the following sizes: $3^3 \times 21$, $5^3 \times 35$ and $8^3 \times 56$, being the results almost independent of the lattice size. This property also holds for bigger values of N.

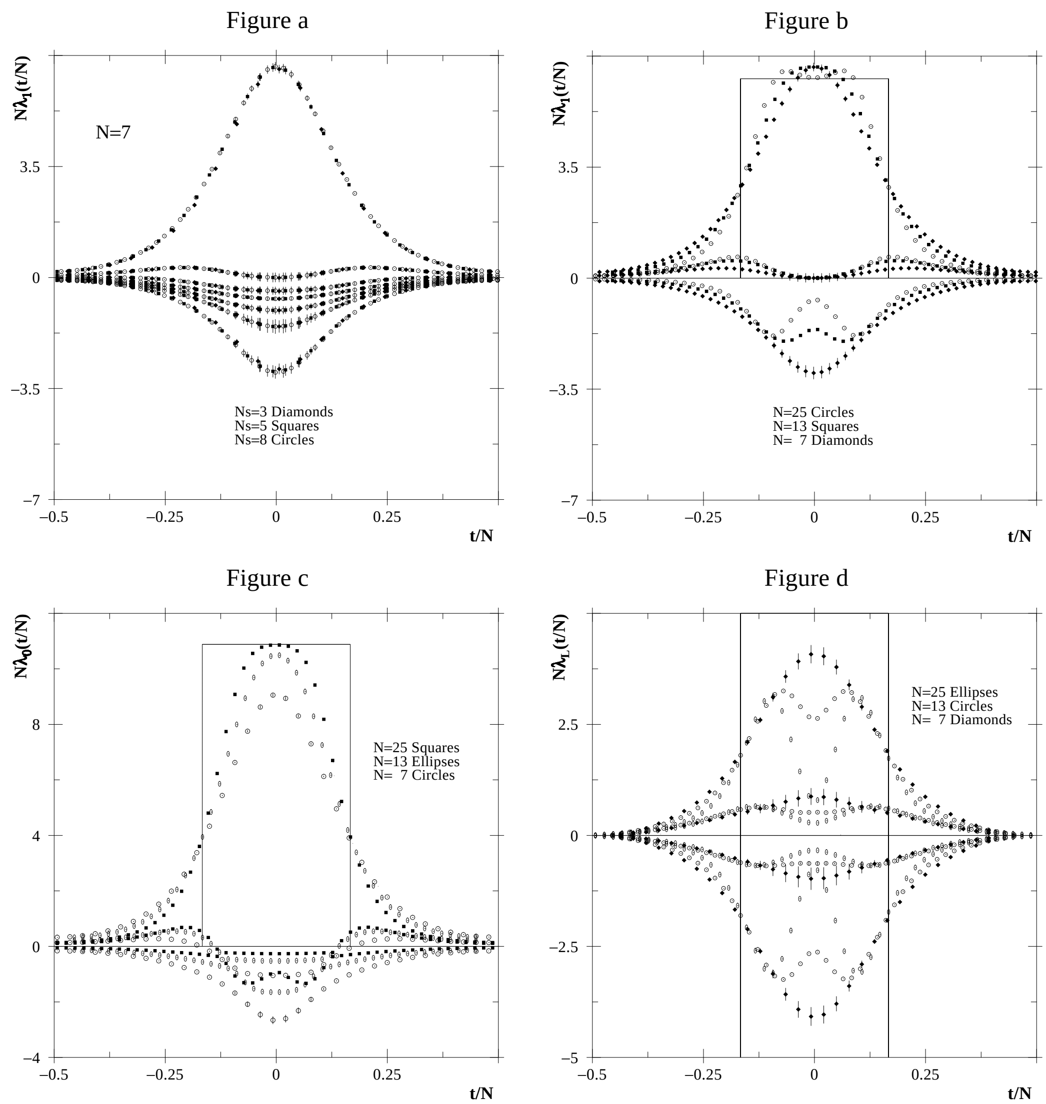

Figure 2: In figure a it is shown the eigenvalues λ_1 of $\mathbf{B}_1$ as a function of time, for the solution with $N = 7$ and different lattice sizes. To compare with the other figures λ_1 is multiplied by N and t divided by N. In figure b we plot the eigenvalues $1, 2$ and N of $\mathbf{B}_1$ multiplied by N as a function of t/N, for three values of N. In figure c the same as in figure b, in this case for $\mathbf{B}_0$. In figure d it is shown the eigenvalues $1, 2, N-1$ and N of $\mathbf{B}_L$ for the same solutions as in figure b.

The behavior with N is shown in figure $2b$ in which we plot the first, second and N-th eigenvalues of $\mathrm{N} \times \mathbf{B}_1$ as a function of t/N for $\mathrm{N} = 7, 13, 25$ and $\vec{k} = (n, n, n)$. The meaning of the points and the error bars is the same as in figure $2a$. The first eigenvalue is approximately independent of N and the other $\mathrm{N}-1$ become degenerate for increasing N. This structure is very similar to the one of the selfdual abelian solution described in appendix A (eqs. (A.14), (A.16) and (A.17)), the first eigenvalue

Sol.	N	a_s	a_t	S_0
I.1	3	0.531(4)	0.389(2)	63.0(2)
I.2	4	0.760(6)	0.484(5)	27.56(12)
I.3	5	1.03(3)	0.583(4)	15.68(12)
I.4	8	2.90(4)	0.980(4)	5.38(2)
I.5	10	6.0(2)	1.535(5)	3.25(1)
II.1	4	0.763(10)	0.480(5)	27.65(12)
II.2	7	1.98(3)	0.814(3)	7.29(4)
II.3	10	6.53(7)	1.51(1)	3.253(7)
II.4	13	19.5(1.5)	5.2(8)	1.7835(7)
II.5	19	290(20)	2.3(2)	0.794(8)
II.6	25	-	2.4(2)	0.448(3)

Table 3: Sizes and heights of the maximum in the action density.

of $N \times B_1$ takes the value $N \times 2\pi/N$ and the other $N-1$ are equal to the value $-N \times 2\pi/(N-1)N$. To compare we plot on figure 2b the first eigenvalue for the abelian solution in the $N \to \infty$ limit, the value 2π for the interval $-1/6 \leq t/N \leq 1/6$. We see that the first eigenvalue of B_i for the solutions with $\vec{k} = (n,n,n)$ are approaching the one of the abelian solution in the N $\to \infty$ limit.

The symmetry properties of the spatial twist vector $\vec{m}$ suggest us to consider the following combinations of B_i fields:

$$\begin{aligned}
\mathbf{B}_0 &= \frac{1}{\sqrt{3}} \left(\mathbf{B}_1 + \mathbf{B}_2 + \mathbf{B}_3\right), \\
\mathbf{B}_L &= \frac{1}{\sqrt{6}} \left(-2\mathbf{B}_1 + \mathbf{B}_2 + \mathbf{B}_3\right), \\
\mathbf{B}_T &= \frac{1}{\sqrt{2}} \left(-\mathbf{B}_2 + \mathbf{B}_3\right)
\end{aligned} \tag{3.13}$$

one parallel to the $\vec{m}$ vector and the other two perpendicular. Also interesting is that, if there is a common component in color space for B_i fields, we will see this component appearing in B_0 and not in B_L and B_T.

In figure 2c we show the first, second and N-th eigenvalues of $N \times \mathbf{B}_0$ as a function of t/N for the same solutions appearing in figure 2b (with the same meaning for points and error bars). We observe the same structure seen in $\mathbf{B}_i$ and the expected property if there is one common component in color space, the dominant eigenvalue is bigger than the one for $\mathbf{B}_i$. We can also observe that this eigenvalue of $N \times \mathbf{B}_0$ is approaching to the shape of the one for the abelian selfdual solution in the $N \to \infty$ limit, in this case $2\pi\sqrt{3}$.

JHEP05(2000)022

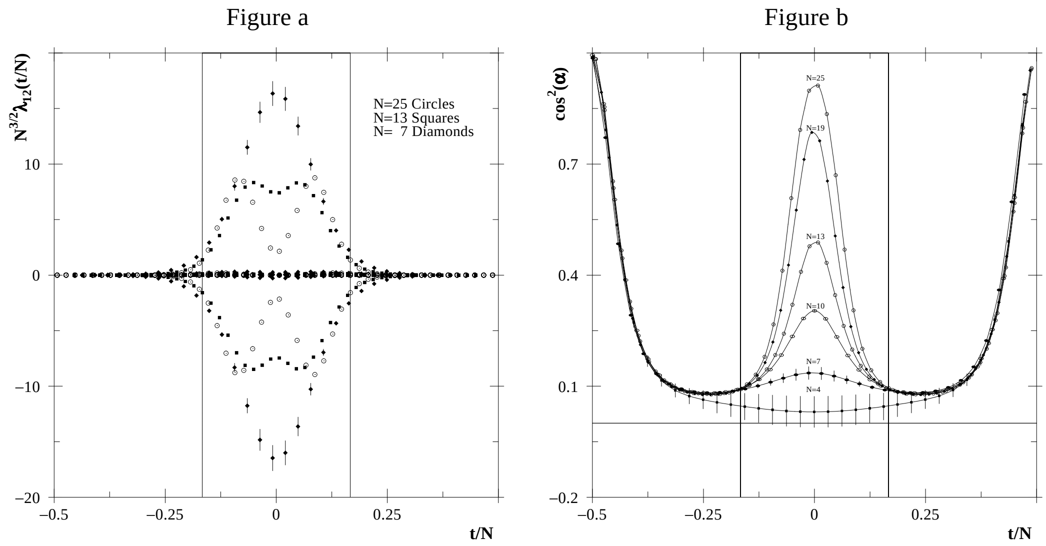

Figure 3: In figure a the eigenvalues λ_{12} of $i[\mathbf{B}_1, \mathbf{B}_2]$ multiplied by $N^{3/2}$ are plotted as a function of t/N for three values of N. In figure b the quantity defined in eq. (3.14) $\cos^2(\alpha_{ij})$ for $i = 1$, $j = 2$ is plotted as a function of t/N for the solutions with $\vec{k} = (n, n, n)$.

In figure $2d$ we show the first, second, (N$-$1)-th and N-th eigenvalues of $N \times \mathbf{B}_L$ as a function of t/N for the same solutions of figure $2b$ (also with the same meaning for points and error bars). The same results are obtained if we show $\mathbf{B}_T$ instead of $\mathbf{B}_L$. The eigenvalue structure is completely different to the ones shown before. In this case the eigenvalues are distributed in pairs, each pair with two opposite values. Another interesting property is that at $t/N = 0$ the eigenvalues go to zero very fast for large N, being $\mathbf{B}_0$ the only one non trivial in this limit.

3.1.5 Colour orientation of the field strength

This is studied by calculating the commutators of $\mathbf{B}_i$'s fields. We show in figure $3a$ the eigenvalues of $N^{3/2}[\mathbf{B}_1, \mathbf{B}_2]$ as a function of $t/$N for the solutions of figures $2b$, $2c$, $2d$ (again the error bars represent spatial dispersion). The same results are obtained if we plot the eigenvalues of $N^{3/2}[\mathbf{B}_2, \mathbf{B}_3]$ or $N^{3/2}[\mathbf{B}_1, \mathbf{B}_3]$ instead of $N^{3/2}[\mathbf{B}_1, \mathbf{B}_2]$. Only two eigenvalues are relevant being the other N $-$ 2 very close to zero. We can see a nice scaling with $N^{3/2}$ of the two relevant eigenvalues at points with $|t|/N > 0.1$, but not at the center of the solution in which the approach to zero is faster. For these quantities the spatial independence for large N also holds.

To study the abelian content of $\mathbf{F}_{\mu\nu}$ we calculate the quantity:

$$\cos^2(\alpha_{ij}) = \frac{\mathrm{tr}(\mathbf{B}_i \mathbf{B}_j)^2}{\mathrm{tr}(\mathbf{B}_i)^2\, \mathrm{tr}(\mathbf{B}_j)^2}\,. \tag{3.14}$$

Whenever $\cos^2(\alpha_{ij}) = 1$ the solution is abelian. In figure $3b$ we plot $\cos^2(\alpha_{12})$ as a function of $t/$N for the solutions with N $= 4, 7, 10, 13, 19, 25$ and $\vec{k} = (n, n, n)$. As in other figures, the points mean the spatial average of the quantity and errors the spatial dispersion. For large N the solutions become abelian at the instanton center (t=0). $\cos^2(\alpha_{ij})$ shows again $\vec{x}$ independence for large N.

For the solutions with $\vec{k}=(1,0,0)$ we obtain the same behavior near the instanton center, but for $T\to\pm\infty$, $\cos^2(\alpha_{ij})$ goes towards a N-depending constant.

3.1.6 Polyakov loops and structure of vacuum

In the gauge we have chosen the relationship between the Polyakov loops and the twist matrices is specially clear. We have $\mathbf{A}_4=0$ and hence the temporal Polyakov loop directly provides the twist matrix $\mathbf{\Omega}_4(\vec{x})$. At $t=-\infty$ $\mathbf{A}_i$ is also fixed to zero and in consequence

$$\mathbf{L}_i(\vec{x},t=-\infty)=\mathbf{\Omega}_i\,. \tag{3.15}$$

Since the spatial twist matrices are constant, compatibility with the spatial boundary conditions for $\vec{m}=(1,1,1)$ (see eq. (1.4)), implies that $\mathrm{N}\mathcal{L}_\mu(t=-\infty)=\mathrm{Tr}(\mathbf{L}_\mu(t=-\infty))=0$. From the boundary conditions in the time direction:

$$\mathcal{L}_i(\vec{x},t=T/2)=\exp\Bigl(ik_i\frac{2\pi}{\mathrm{N}}\Bigr)\mathcal{L}_i(\vec{x},t=-T/2)\,, \tag{3.16}$$

it is clear that also at $t=\infty$ the spatial Polyakov loops are zero. To characterize the vacuum states between which the configurations interpolate we need thus an additional quantity provided by $\mathrm{N}\mathcal{L}_{zyx}=\mathrm{Tr}(\mathbf{L}_z\mathbf{L}_y\mathbf{L}_x)$. Using the twist matrices given in eq. (3.5) the values for $\mathcal{L}_{zyx}$ in a vacuum are,

$$\mathcal{L}_{zyx}=\exp\left(\frac{\imath 2\pi p}{\mathrm{N}}\right)\,, \tag{3.17}$$

where p takes the values $p=1,\ldots,\mathrm{N}$. There are therefore N different vacua labeled by the value of $\mathcal{L}_{zyx}$. Our solutions interpolate between two of them as can be seen from the boundary condition in the time direction for $\mathcal{L}_{zyx}$:

$$\mathcal{L}_{zyx}(x_j,t=T/2)=\exp\Bigl(\imath\sum_i k_i\frac{2\pi}{\mathrm{N}}\Bigr)\mathcal{L}_{zyx}(x_j,t=-T/2)\,. \tag{3.18}$$

We can parametrize the data obtained for $\mathcal{L}_i$, $\mathcal{L}_0$, $\mathcal{L}_{zyx}$ as,

$$\mathcal{L}_i(x_{j\neq i},t)\;=\;f_i(t)e^{i\alpha_i(t)}\exp\left\{\frac{i2\pi}{\mathrm{N}}(\vec{m}\times\vec{r})_i\right\}, \tag{3.19}$$

$$\mathcal{L}_0(\vec{x})\;=\;Ae^{i\alpha_0}\exp\left\{\frac{-i2\pi}{\mathrm{N}}\vec{k}\vec{r}\right\}, \tag{3.20}$$

$$\mathcal{L}_{zyx}(\vec{x},t)\;=\;f_{zyx}(t)e^{i\alpha_{zyx}(t)}\,, \tag{3.21}$$

note that with the gauge fixing condition for the Polyakov loops those functions take the values: $\alpha_0=\pi$, $\alpha_i(t=0)=\pi$ ($\vec{r}=\vec{0}$ is the maximum of the solution).

JHEP05(2000)022

Sol.	N	A	$\frac{10^4\chi^2}{N_s^3}$	B	w	$\frac{10^3\chi^2}{N_t}$	A_{zyx}	w_{zyx}	v_{zyx}	$\frac{10^4\chi^2}{N_s^3\times N_t}$
I.1	3	0.453	334.1	0.657	8.04	0.0188	2.057	15.77	20.52	13.898
I.2	4	0.472	75.41	0.764	8.20	0.0125	2.093	15.79	16.87	0.5014
I.3	5	0.485	12.96	0.846	8.22	0.0077	2.099	15.64	15.70	0.4166
I.4	8	0.504	0.4252	0.969	8.35	0.0221	2.095	15.93	14.88	0.0411
I.5	10	0.508	0.0094	0.998	7.98	0.0214	2.092	16.02	14.60	0.0375
II.1	4	0.288	0.2311	0.763	8.11	0.0534	2.094	15.82	16.88	0.4846
II.2	7	0.150	0.0017	0.929	8.11	0.0025	2.099	15.94	15.07	0.0868
II.3	10	0.102	$< 10^{-6}$	0.999	8.19	0.0334	2.093	16.19	14.70	0.0353
II.4	13	0.078	$< 10^{-6}$	1.029	8.05	0.0925	2.095	16.53	14.52	0.0428
II.5	19	0.053	$< 10^{-6}$	1.057	7.96	0.2738	2.103	17.07	14.32	0.0425
II.6	25	0.040	$< 10^{-6}$	1.066	7.88	0.4323	2.123	17.45	14.21	0.0389

Table 4: Results of the fits to eqs. (3.20), (3.22) and (3.23).

For $\mathcal{L}_i$ we make a fit at each temporal point to the spatial dependence of eq. (3.19). The values of $\sqrt{\chi^2/{N_s}^3}$ obtained for the solutions with temporal twist vector $\vec{k} = (n,n,n)$ are always smaller than 1.24^o, 0.27^o, 0.07^o and 0.004^o for the values $N = 4, 7, 10$ and 13 respectively. For the solutions with temporal twist vector $\vec{k} = (1,0,0)$ these values are 2.7^o, 1.28^o, 0.81^o, 0.13^o and 0.05^o for $N = 3, 4, 5, 8$ and 10, respectively. We extract the values of $\mathcal{L}_i$ at the spatial maximum of the solution and make a fit to the expression:

$$f_i(t) = \frac{B}{N}\cosh\left(\frac{wt}{N}\right), \tag{3.22}$$

the values of B and w are given in table 4.

The functions f_{zyx}, $\alpha_{zyx}^{(1,0,0)}$ and $\alpha_{zyx}^{(n,n,n)}$ parametrizing $\mathcal{L}_{zyx}$ in equation 3.21 are well fitted by:

$$\begin{aligned} f_{zyx}(t) &= 1 - \frac{A_{zyx}}{N\cosh(w_{zyx}t/N)} \\ \alpha_{zyx}^{(1,0,0)}(t) &= \frac{\pi}{N}\left(1 + \tanh\left(v_{zyx}\frac{t}{N}\right)\right), \\ \alpha_{zyx}^{(n,n,n)}(t) &= \frac{\pi}{N}\left(1 - \tanh\left(v_{zyx}\frac{t}{N}\right)\right) \end{aligned} \tag{3.23}$$

the values obtained for A_{zyx}, w_{zyx}, v_{zyx} are given in table 4. And finally $\mathcal{L}_0$ only needs the constant A to be fitted, their values are given in table 4.

We compare our results with the Polyakov loops for the abelian selfdual solution described in appendix A,

$$\mathcal{L}_i(x_{j\neq i},t) = \frac{1}{N}e^{i\pi}\,\mathrm{Exp}\left(i\frac{2\pi}{N}\frac{N-1}{3}\frac{t}{T}\right)\mathrm{Exp}\left(i\frac{2\pi}{N}(\vec{m}\times\vec{x})_i\right),$$
$$\mathcal{L}_0(\vec{x}) = \frac{1}{N}e^{i\pi}\,\mathrm{Exp}\left\{\frac{-i2\pi}{\mathrm{N}}\vec{k}\vec{x}\right\},$$

where $-T/2 \leq t \leq T/2$ and $-0.5 \leq x_i \leq 0.5$. We can see that the Polyakov loops in the $N \to \infty$ limit for the solutions with $\vec{k} = (n,n,n)$ are the same as the ones for the abelian selfdual solution.

3.2 Gauge-dependent quantities

3.2.1 Eigenvalues of $\mathbf{A}_i$

After gauge fixing to the gauge described previously, we calculate the eigenvalues of $\mathbf{A}_i$. The main properties of these quantities are shown in figures $4a$, $4b$, $4c$ and $4d$. We only show the results for the solutions with twist $\vec{k} = (n,n,n)$, because the same figures are obtained for the solutions with twist $\vec{k} = (1,0,0)$ changing the sign of the gauge field, $\mathbf{A}_i \to -\mathbf{A}_i$.

In figure $4a$ we show how the eigenvalues of $\mathbf{A}_1$ scale towards the continuum limit. We plot these quantities for the solutions with $N = 7$, temporal twist vector $\vec{k} = (2,2,2)$ and lattice sizes $3^3 \times 21$, $5^3 \times 35$ and $8^3 \times 56$. As in previous figures, points values are the spatial average of the eigenvalues and error bars mean spatial dispersion. We can see that the discretization errors still are important for the solution with size $N_s = 3$ but are very small for bigger sizes. For these quantities we consider in the following lattice sizes with $N_s \geq 4$.

The behavior with N is shown in figure $4b$ in which we plot the first, second and N-th eigenvalues of $\mathbf{A}_1$ as a function of t/N for $\mathrm{N} = 7, 10, 13$ and $\vec{k} = (n,n,n)$ (points and error bars have the same meaning as before). Very similar results are obtained if we plot $\mathbf{A}_2$ or $\mathbf{A}_3$ instead of $\mathbf{A}_1$. One of the eigenvalues is approximately independent of N and the other N-1 become degenerate and approach zero for increasing N. We also show the biggest eigenvalue for the abelian selfdual solution described in section A.3 of appendix A in the $N \to \infty$ limit. In this limit the function describing this eigenvalue is $2\pi(t/N + 1/6)$ for the values $-1/6 \leq t/N \leq 1/6$. We can see that the first eigenvalue of A_1 is approaching the one of the abelian selfdual solution in the $N \to \infty$ limit.

As for $\mathbf{B}_i$ fields, we consider the following combinations of $\mathbf{A}_i$ fields,

$$\begin{aligned}
\mathbf{A}_0 &= \frac{1}{\sqrt{3}}\left(\mathbf{A}_1 + \mathbf{A}_2 + \mathbf{A}_3\right),\\
\mathbf{A}_L &= \frac{1}{\sqrt{6}}\left(-2\mathbf{A}_1 + \mathbf{A}_2 + \mathbf{A}_3\right),\\
\mathbf{A}_T &= \frac{1}{\sqrt{2}}\left(-\mathbf{A}_2 + \mathbf{A}_3\right).
\end{aligned} \tag{3.24}$$

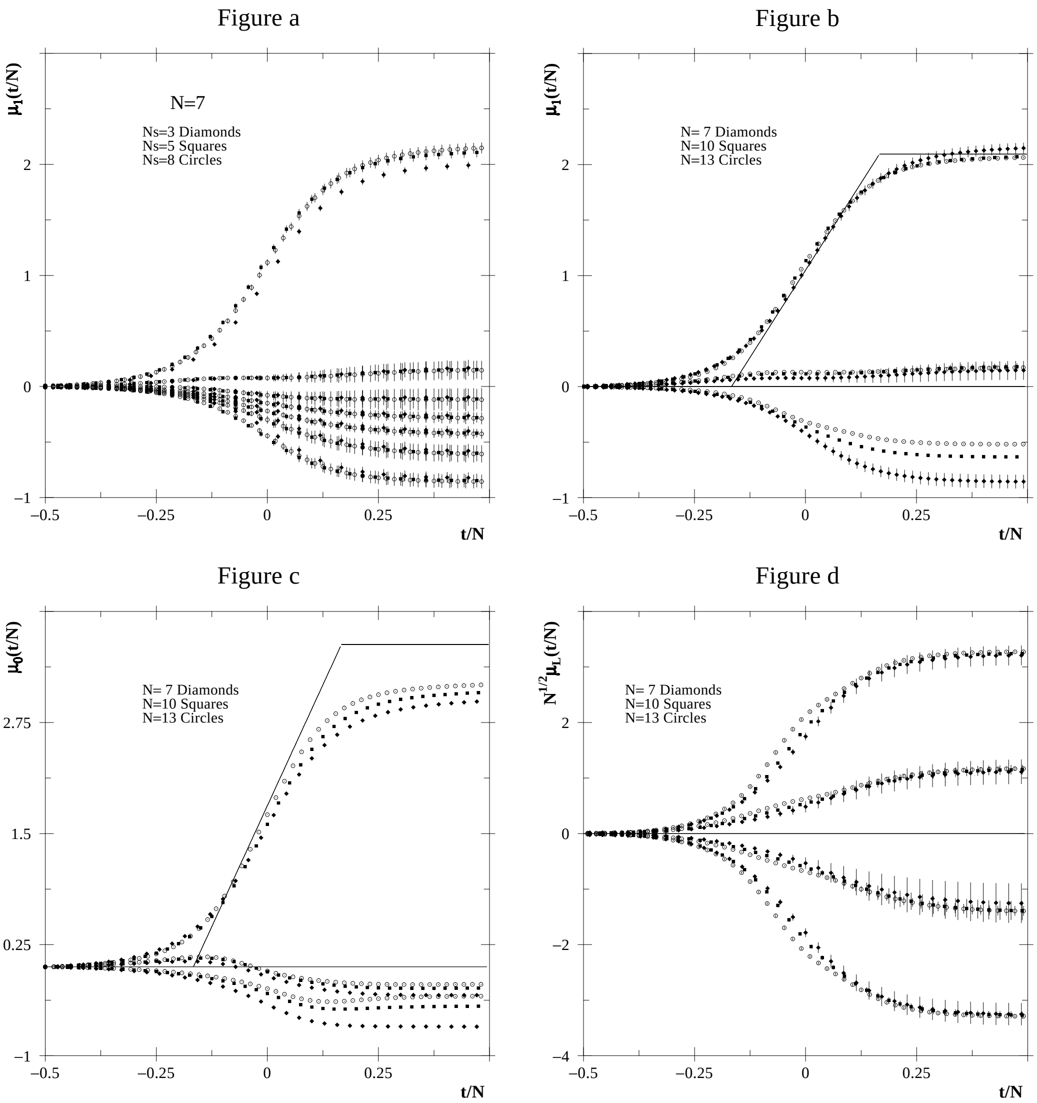

Figure 4: In figure a we show the eigenvalues μ_1 of $\mathbf{A}_1$ as a function of time for the solution with $N = 7$ and different lattice sizes. In figure b it is plotted the eigenvalues $1, 2$ and N of $\mathbf{A}_1$ as a function of t/N, for three different values of N. In figure c the eigenvalues $1, 2$ and N of $\mathbf{A}_0$ are plotted as a function of t/N. In figure d the eigenvalues $1, 2, N-1$ and N of $\mathbf{A}_L$ multiplied by $\sqrt{N}$ are plotted as a function of t/N for the same solutions shown in figure b.

In figure 4c we show the first, second and N-th eigenvalues of $\mathbf{A}_0$ for the same solutions appearing in figure 4b (points and error bars have the same meaning as before). We observe that the eigenvalue structure is the same one seen for $\mathbf{A}_1$ and the expected result if there is a common component in color space for $\mathbf{A}_1$, $\mathbf{A}_2$ and $\mathbf{A}_3$, the first eigenvalue of $\mathbf{A}_0$ is bigger than the first one for $\mathbf{A}_i$. We also show the first eigenvalue of $\mathbf{A}_0$ for the abelian selfdual solution in the N $\to \infty$ limit, in this case the function $2\pi\sqrt{3}(t/N + 1/6)$ for points $-1/6 \leq t/N \leq 1/6$. The first eigenvalue of

JHEP05(2000)022

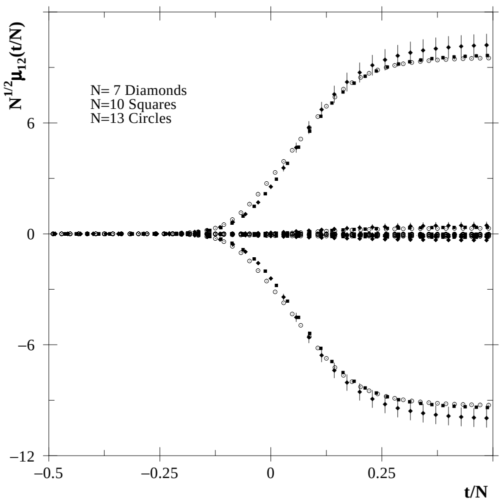

Figure 5: In this figure we plot the eigenvalues μ_{12} of $\imath[\mathbf{A}_1, \mathbf{A}_2]$ multiplied by $N^{1/2}$ as a function of t/N for three values of N.

A_0 is approaching the one of the abelian selfdual solution in the $N \to \infty$ limit.

In figure 4d we show the first, second, $(N-1)$-th and N-th eigenvalues of $\sqrt{N} \times \mathbf{A}_L$ for the same solutions appearing in figure 4b (points and error bars have the same meaning as before). Very similar results are obtained if we plot the eigenvalues of $\mathbf{A}_T$ instead of the ones for $\mathbf{A}_L$. The eigenvalue structure is completely different to the one shown for $\mathbf{A}_0$, $\mathbf{A}_i$. The eigenvalues are distributed in pairs, each pair with two opposite values. As can be seen from the figure these eigenvalues goes to zero as $1/\sqrt{N}$. This means that $\mathbf{A}_L$ and $\mathbf{A}_T$ go to zero for large N while $\mathbf{A}_0$ is independent of N.

3.2.2 Colour orientation of the potential

As for the field strength, this is studied by calculating the commutators of $\mathbf{A}_i$'s fields. We show in figure 5 the eigenvalues of $N^{1/2}[\mathbf{A}_1, \mathbf{A}_2]$ as a function of $t/$N for the solutions of figures 4b, 4c and 4d (again the error bars represent spatial dispersion). Only two eigenvalues are relevant being the other N $-$ 2 very close to zero and it is also clear the scaling with $N^{1/2}$ of the two relevant eigenvalues. From this figure we conclude that the gauge field $\mathbf{A}_i$ become abelian in the large-N limit, compatible with the properties presented before, $\mathbf{A}_0$ is the remaining component in this limit while $\mathbf{A}_L$, $\mathbf{A}_T$ goes to zero with $N^{1/2}$.

3.2.3 Twist matrix Ω_4

The temporal twist matrix behaves very differently depending of the temporal twist used. Note that their trace is the temporal Polyakov loop given before. We study their eigenvalues and obtain the following. For temporal twist $\vec{k} = (n, n, n)$ we fit the eigenvalues to the expression:

$$
\begin{aligned}
\lambda_j &= \mathrm{Exp}\left(\frac{\imath 2\pi\vec{k}\vec{r}}{N(N-1)} + \imath\frac{\pi}{3} + \imath N\pi\right), \quad j = 1, \ldots, (N-1)/3\,, \\
\lambda_j &= \mathrm{Exp}\left(\frac{\imath 2\pi\vec{k}\vec{r}}{N(N-1)} + \imath\pi + \imath N\pi\right), \quad j = (N-1)/3+1, \ldots, 2(N-1)/3\,, \\
\lambda_j &= \mathrm{Exp}\left(\frac{\imath 2\pi\vec{k}\vec{r}}{N(N-1)} + \imath\frac{5\pi}{3} + \imath N\pi\right), \quad j = 2(N-1)/3+1, \ldots, N-1\,, \\
\lambda_N &= \mathrm{Exp}\left(-\frac{i2\pi\vec{k}\vec{r}}{N} + i\pi\right).
\end{aligned} \tag{3.25}
$$

This expression was obtained from the numerical data for the eigenvalues of the twist matrix $\mathbf{\Omega_4}$. This is a good parametrization for all values of N studied ($N = 4, 7, 10, 13, 19, 25$) and the fits to this expression are better for bigger values of N. The interesting point is that this expression for the eigenvalues is the one for the eigenvalues of the twist matrix $\mathbf{\Omega_4}$ given in (A.17) for the abelian solution described in appendix A.

For temporal twist $\vec{k} = (1,0,0)$ we obtain for large N that the eigenvalues only depend on the x_1 coordinate, but we have not found a good parametrization in this case.

4. Conclusions

In this paper we have presented a set of solutions of the SU(N) Yang-Mills equations of motion. These solutions are selfdual or antiselfdual, have fractional topological charge $Q = 1/N$ and live on the four-dimensional torus, T^4. We have studied the case when the lengths of the torus are $L^3 \times T$ with $T \gg L$ and with twist vectors $\vec{m} = (1,1,1)$ and $\vec{k} = \frac{N-1}{3}(1,1,1)$, $\vec{k} = (1,0,0)$. Now we summarize the main results we have obtained.

The obtained results show a clear tendency to describe continuum functions, being the different lattice sizes used enough to observe independence of the number of lattice points. This property indicates that the obtained configurations describe continuum Yang-Mills fields.

For each value of N and twist we always obtain the same solution up to a gauge transformation and a spatial translation. This means that we can repeat the procedure to obtain another configuration and the differences observed will be a gauge transformation and a spatial translation.

The main characteristic of the solutions are the following:

- The obtained solutions are selfdual or antiselfdual in all the studied cases. We observe numerically that this property is satisfied with a very high precision. This guarantees that these configurations are solutions of the equations of motion.

- The size of the solutions is approximately $N/3$. By size we understand the length of the region in the temporal direction in which the core of the solution is included. We can see this property in all quantities shown in section 3. e.g. we can look at the energy profile and check that the most relevant part is located in a region of size $\sim N/3$. Also in the same region the eigenvalues of the field strength take their maximum values and go to zero out of this zone. We can say similar assertions for all quantities calculated in this paper.

- The action density has only one maximum for values of $N \leq 13$ and a double peak structure for bigger values. The spatial dependence of the action density disappears with increasing N being only dependent of the temporal coordinate.

- The orientation of the field strength $\mathbf{F}_{\mu\nu}$ in color space is very dependent on the value of N. For smaller values of N the different components of $\mathbf{F}_{\mu\nu}$ are built from different components in color space while for bigger values of N the same component in color space gives the main contribution to the field strength. This property also holds for the gauge field $\mathbf{A}_\mu$. This means that, in the $N \to \infty$ limit, these solutions are abelians.

- In the $N \to \infty$ limit one eigenvalue gives the most important contribution to some quantities calculated in this article. In this limit, each component of the field strength $\mathbf{F}_{\mu\nu}$ has one eigenvalue which is approximately N times bigger than the other $N-1$ eigenvalues. This property also holds for each component of the gauge field $\mathbf{A}_\mu$.

- Independence of the temporal twist vector $\vec{k}$ for some of the calculated quantities. This is an N-independent property which holds when the length in the temporal direction goes to ∞. This property can be seen, for example, in the field strength $\mathbf{F}_{\mu\nu}$; if we change the temporal twist vectors used, $\vec{k}_1 = (1, 0, 0)$ and $\vec{k}_2 = (n, n, n)$ we obtain that $\mathbf{B}_\mathbf{i}^{\vec{\mathbf{k}}_1} = \mathbf{B}_\mathbf{i}^{\vec{\mathbf{k}}_2}$ and $\mathbf{E}_\mathbf{i}^{\vec{\mathbf{k}}_1} = -\mathbf{E}_\mathbf{i}^{\vec{\mathbf{k}}_2}$. A similar property is held for the gauge field, under the change of the twist vectors we obtain the relation $\mathbf{A}_\mathbf{i}^{\vec{\mathbf{k}}_1} = -\mathbf{A}_\mathbf{i}^{\vec{\mathbf{k}}_2}$.

We have not succeeded in finding an analytic expression describing the properties of the studied solutions. Obviously, the first requirement for an ansatz prepared to find the analytical expression is that this ansatz satisfies the previously shown properties. The most promising approach seems to be an ansatz based on the similarity of the solution in the large-N limit with the abelian solution presented in appendix A. Nevertheless, if the solutions in this limit coincide with the abelian solution, something singular must happen at points $|t/N| = 1/6$, being therefore not ease to use

JHEP05(2000)022

this similarity to find the analytic expression. To conclude, we hope that all the numerical data presented will be helpful for other attempts to find the analytical expression of the solutions presented in this paper.

A. Analytic solutions

A.1 't Hooft construction

The $\mathbf{A}_\mu$ and $\mathbf{F}_{\mu\nu}$ fields are built from a diagonal matrix $\mathbf{T}$, in the following way:

$$\mathbf{A}_\mu(x) = -\frac{\pi}{N}\sum_\nu \frac{\alpha_{\mu\nu}x_\nu}{l_\mu l_\nu}\mathbf{T}\,, \qquad \mathbf{F}_{\mu\nu}(x) = \frac{2\pi}{N}\frac{\alpha_{\mu\nu}}{l_\mu l_\nu}\mathbf{T}\,, \tag{A.1}$$

where $\alpha_{\mu\nu}$ is an antisymmetric tensor and l_μ the length of the torus in the μ direction. The matrix $\mathbf{T}$ has the form

$$\mathbf{T} = \begin{pmatrix} -l\mathbb{1}_{k\times k} & \mathbf{0}_{k\times l} \\ \mathbf{0}_{l\times k} & k\mathbb{1}_{l\times l} \end{pmatrix}, \tag{A.2}$$

being k and l integer numbers ($k+l=N$). To build the twist matrices we use the $\mathbf{P}$ and $\mathbf{Q}$ matrices defined in eq. (3.6). From these matrices we construct another set of matrices,

$$\mathbf{P}_1, \mathbf{Q}_1 = \begin{pmatrix} (\mathbf{P},\mathbf{Q})_{k\times k} & \mathbf{0}_{k\times l} \\ \mathbf{0}_{l\times k} & \mathbb{1}_{l\times l} \end{pmatrix}; \qquad \mathbf{P}_2, \mathbf{Q}_2 = \begin{pmatrix} \mathbb{1}_{k\times k} & \mathbf{0}_{k\times l} \\ \mathbf{0}_{l\times k} & (\mathbf{P},\mathbf{Q})_{l\times l} \end{pmatrix} \tag{A.3}$$

satisfying the properties,

$$\begin{aligned} \mathbf{P}_1\mathbf{Q}_1 &= \mathbf{Q}_1\mathbf{P}_1 \,\mathrm{Exp}\left\{\frac{i2\pi}{N}\left(\mathbb{1} - \frac{\mathbf{T}}{k}\right)\right\}; \\ \mathbf{P}_2\mathbf{Q}_2 &= \mathbf{Q}_2\mathbf{P}_2 \,\mathrm{Exp}\left\{\frac{i2\pi}{N}\left(\mathbb{1} + \frac{\mathbf{T}}{l}\right)\right\}. \end{aligned} \tag{A.4}$$

And the ansatz for the twist matrices is,

$$\mathbf{\Omega}_\mu(x) = \mathbf{P}_1^{s_\mu}\mathbf{Q}_1^{t_\mu}\mathbf{P}_2^{u_\mu}\mathbf{Q}_2^{v_\mu}\ \mathrm{Exp}\left\{-\frac{i\pi}{N}\sum_\nu \frac{\alpha_{\mu\nu}x_\nu}{l_\nu}\mathbf{T}\right\}, \tag{A.5}$$

where s_μ, t_μ, u_μ and v_μ are arbitrary integer numbers. These matrices must satisfy the consistency condition,

$$\mathbf{\Omega}_\mu(x_\nu + l_\nu)\mathbf{\Omega}_\nu(x_\mu) = \mathbf{\Omega}_\nu(x_\mu + l_\mu)\mathbf{\Omega}_\mu(x_\nu)\ \mathrm{Exp}\left(-\frac{i2\pi n_{\mu\nu}}{\mathrm{N}}\right). \tag{A.6}$$

This condition imposes the following equations for s_μ, t_μ, u_μ and v_μ:

$$\begin{aligned} \frac{1}{k}(t_\mu s_\nu - t_\nu s_\mu) &= l\frac{\alpha_{\mu\nu}}{N} + \frac{n_{\mu\nu}}{N} + A_{\mu\nu}\,; \\ \frac{1}{l}(v_\mu u_\nu - v_\nu u_\mu) &= -k\frac{\alpha_{\mu\nu}}{N} + \frac{n_{\mu\nu}}{N} + B_{\mu\nu}\,, \end{aligned} \tag{A.7}$$

where $A_{\mu\nu}$ and $B_{\mu\nu}$ are integer numbers. To solve these two equations we give to $\alpha_{\mu\nu}$ and $n_{\mu\nu}$ the form,

$$n_{\mu\nu} = n^{(1)}_{\mu\nu} + n^{(2)}_{\mu\nu}\,; \qquad \alpha_{\mu\nu} = \frac{n^{(1)}_{\mu\nu}}{k} - \frac{n^{(2)}_{\mu\nu}}{l} \tag{A.8}$$

and then equations in formula (A.7) are transformed to,

$$n^{(1)}_{\mu\nu} = t_\mu s_\nu - t_\nu s_\mu + kA_{\mu\nu}\,; \qquad n^{(2)}_{\mu\nu} = v_\mu u_\nu - v_\nu u_\mu + lB_{\mu\nu}\,, \tag{A.9}$$

which can be solved if the following condition is satisfied,

$$n^{(1)}_{\mu\nu}\tilde{n}^{(1)}_{\mu\nu} = 0 \bmod k\,; \qquad n^{(2)}_{\mu\nu}\tilde{n}^{(2)}_{\mu\nu} = 0 \bmod l\,. \tag{A.10}$$

The $n^{(1)}_{\mu\nu}$ and $n^{(2)}_{\mu\nu}$ tensors are orthogonal twist tensors for a SU(k) and SU(l) group, respectively.

The topological charge for these solutions is,

$$Q = \frac{1}{N}\frac{\alpha_{\mu\nu}\tilde{\alpha}_{\mu\nu}}{4}kl = \frac{1}{N}\left(\vec{k}^{(1)}\vec{m}^{(1)}\frac{l}{k} + \vec{k}^{(2)}\vec{m}^{(2)}\frac{k}{l} - \vec{k}^{(1)}\vec{m}^{(2)} - \vec{k}^{(2)}\vec{m}^{(1)}\right), \tag{A.11}$$

where we have defined the vectors ${k_i}^{(n)} = {n_{0i}}^{(n)}$, ${m_i}^{(n)} = \epsilon_{ijk}{n_{jk}}^{(n)}/2$, with $n = 1, 2$.

A.2 Some examples

Now we give some examples of solutions built using 't Hooft construction, and for the torus lengths used in this article: $l_x = l_y = l_z = 1$ and $l_t \to \infty$. In fact, our examples will be given for any value of l_t. The topological charge in our examples is given by eq. (A.11) and the action by the following equation:

$$\begin{aligned} S = \frac{8\pi^2}{N}\frac{1}{2}\Bigg\{ &\frac{1}{l_t}\left(\vec{k}^{(1)}\vec{k}^{(1)}\frac{l}{k} + \vec{k}^{(2)}\vec{k}^{(2)}\frac{k}{l} - 2\vec{k}^{(1)}\vec{k}^{(2)}\right) + \\ &+ l_t\left(\vec{m}^{(1)}\vec{m}^{(1)}\frac{l}{k} + \vec{m}^{(2)}\vec{m}^{(2)}\frac{k}{l} - 2\vec{m}^{(1)}\vec{m}^{(2)}\right)\Bigg\}. \end{aligned} \tag{A.12}$$

The minimum value for the action, $S = 8\pi^2|Q|$, is obtained when the solution is selfdual or antiselfdual. This condition imposes a value for the temporal length l_t, obtained solving the equation,

$$\frac{\vec{k}^{(1)}}{l} - \frac{\vec{k}^{(2)}}{k} = \pm l_t\left(\frac{\vec{m}^{(1)}}{l} - \frac{\vec{m}^{(2)}}{k}\right), \tag{A.13}$$

the positive sign for selfdual solutions and the negative sign for antiselfdual solutions. Now we give some examples for the twist vectors used in this article:

1. Solutions for twist vectors $\vec{m} = (1,1,1)$ and $\vec{k} = (n,n,n)$, with $N = 3n+1$ for $n = 1,2,3,\ldots$ We choose $k = N-1$ and $l = 1$ and the twist vectors in subspaces SU(k) and SU(l) as,

$$\vec{m}^{(1)} = (1,1,1)\ \vec{k}^{(1)} = (n,n,n)\,; \qquad \vec{m}^{(2)} = (0,0,0)\ \vec{k}^{(2)} = (0,0,0)\,.$$

The topological charge for this solution is $Q = 1/N$ and it is selfdual when $l_t = n$.

2. Solutions for twist vectors $\vec{m} = (1,1,1)$ and $\vec{k} = (1,0,0)$. We choose the twist vectors in SU(k) and SU(l) subspaces as,

$$\vec{m}^{(1)} = (1,1,1)\ \vec{k}^{(1)} = (0,0,0)\,; \qquad \vec{m}^{(2)} = (0,0,0)\ \vec{k}^{(2)} = (1,0,0)\,.$$

This choice works for any values of k, l. The topological charge for this solution is $Q = -1/N$ and in this case it is not possible to solve the selfduality equation.

A.3 Changing the gauge

Now we change the gauge for one of the solutions described before to the gauge used in section 3. We choose the solution given in example 1. In this case $k = N-1$, $l = 1$, $n^{(1)}_{\mu\nu} = n_{\mu\nu}$ and $n^{(2)}_{\mu\nu} = 0$. The fields are,

$$\mathbf{A}_\mu(x) = -\frac{\pi}{N(N-1)}\sum_\nu \frac{n_{\mu\nu}x_\nu}{l_\mu l_\nu}\mathbf{T}\,, \qquad \mathbf{F}_{\mu\nu}(x) = \frac{2\pi}{N(N-1)}\frac{n_{\mu\nu}}{l_\mu l_\nu}\mathbf{T}\,. \tag{A.14}$$

We remember that the torus lengths were $l_x = l_y = l_z = 1$ and l_t can take any value, and the twist vectors were $\vec{m} = (1,1,1)$ and $\vec{k} = (n,n,n)$, with $N = 3n+1$. The action and the topological charge take the values,

$$S = \frac{8\pi^2}{N}\frac{1}{2}\left(\frac{l_t}{n} + \frac{n}{l_t}\right), \qquad Q = \frac{1}{N}$$

the twist matrices are,

$$\mathbf{\Omega}_\mu(x) = \mathbf{P}_1^{s_\mu}\mathbf{Q}_1^{t_\mu}\,\mathrm{Exp}\left\{-\frac{i\pi}{N(N-1)}\sum_\nu \frac{n_{\mu\nu}x_\nu}{l_\nu}\mathbf{T}\right\} \tag{A.15}$$

and the values for s_μ, t_μ,

$$\begin{aligned} s_1 &= 0\,, \qquad s_2 = 1\,, \qquad s_3 = N-2\,, \qquad s_4 = \frac{2(N-1)}{3}\,, \\ t_1 &= 1\,, \qquad t_2 = 0\,, \qquad t_3 = N-2\,, \qquad t_4 = \frac{N-1}{3}\,. \end{aligned}$$

The gauge used in section 3 is: $\mathbf{A}_4 = 0$ and $\mathbf{A}_i(t = -\infty) = 0$. For our example we can not use the same gauge because t is finite and $\mathbf{F}_{\mu\nu} \neq 0$ for any value of t (this is the condition needed to put $A_i(t) = 0$ at some point t). The most similar gauge condition is the following one:

$$\mathbf{A}_4 = 0\,, \quad \mathbf{A}_3(t=0) = 0\,, \quad \mathbf{A}_2(t=0, z=0) = 0\,, \quad \mathbf{A}_1(t=0, z=0, y=0) = 0$$

because all links associated with these fields were rotated to the identity. The field $\mathbf{A}_\mu$ and the twist matrices in this gauge are,

$$\begin{aligned}
\mathbf{A}_4 &= 0\,, \qquad \mathbf{A}_3 = \frac{2\pi}{N(N-1)}\mathbf{T}\frac{n}{l_t}t\,, \\
\mathbf{A}_2 &= \frac{2\pi}{N(N-1)}\mathbf{T}\Big(\frac{n}{l_t}t - z\Big)\,, \\
\mathbf{A}_1 &= \frac{2\pi}{N(N-1)}\mathbf{T}\Big(\frac{n}{l_t}t + z - y\Big)\,,
\end{aligned} \tag{A.16}$$

$$\begin{aligned}
\mathbf{\Omega}_4 &= \mathbf{P}_1{}^{s_4}\mathbf{Q}_1{}^{t_4}\,\mathrm{Exp}\left\{-i\frac{2\pi}{N(N-1)}\mathbf{T}\vec{k}\vec{r}\right\}\,, \\
\mathbf{\Omega}_3 &= \mathbf{P}_1{}^{s_3}\mathbf{Q}_1{}^{t_3}\,\mathrm{Exp}\left\{i\frac{2\pi}{N(N-1)}\mathbf{T}(y-x)\right\}\,, \\
\mathbf{\Omega}_2 &= \mathbf{P}_1{}^{s_2}\mathbf{Q}_1{}^{t_2}\,\mathrm{Exp}\left\{i\frac{2\pi}{N(N-1)}\mathbf{T}x\right\}\,, \qquad \mathbf{\Omega}_1 = \mathbf{P}_1{}^{s_1}\mathbf{Q}_1{}^{t_1}\,.
\end{aligned} \tag{A.17}$$

We compare along section 3 the results obtained for large values of N with this solution (with $l_t = n$) because some properties are very similar for both solutions in this limit.

Finally, we give the value of the Polyakov loops for this example,

$$\mathcal{L}_\mu = \frac{1}{N}\,\mathrm{Exp}\left(-i\frac{2\pi}{N}\sum_\nu \frac{n_{\mu\nu}x_\nu}{l_\nu}\right)\,,$$

note that this quantity is gauge invariant and could be calculated with the two different $\mathbf{A}_\mu$ given before, obtaining the same result.

Acknowledgments

The results presented in this article are part of the Ph.D. Thesis of the author [22]. Most of the ideas developed in this work come from suggestions and fruitful discussions with Antonio González-Arroyo. I also acknowledge useful discussions with Margarita García Pérez and Carlos Pena. This work has been supported by the Spanish Ministerio de Educación y Cultura under a postdoctoral Fellowship and by CICYT under grant AEN97-1678.

References

[1] G. 't Hooft, *A property of electric and magnetic flux in nonabelian gauge theories*, *Nucl. Phys.* **B 153** (1979) 141; *Confinement and topology in non-abelian gauge theories*, *Acta Phys. Austriaca, Suppl.* **XXII** (1980) 531.

[2] A. González-Arroyo, *Yang-Mills fields on the 4-dimensional torus*, in *Advanced school for nonperturbative quantum field physics*, M. Asorey and A. Dobado eds. 1998, p. 57.

[3] P. van Baal, *Some results for* SU(N) *gauge fields on the hypertorus*, *Comm. Math. Phys.* **85** (1982) 529.

[4] G. 't Hooft, *Some twisted selfdual solutions for the Yang-Mills equations on a hypertorus*, *Comm. Math. Phys.* **81** (1981) 267.

[5] M.G. García Pérez, A. González-Arroyo and B. Soderberg, *Minimum action solutions for* SU(2) *gauge theory on the torus with nonorthogonal twist*, *Phys. Lett.* **B 235** (1990) 117.

[6] M. García Pérez and A. González-Arroyo, *Numerical study of yang-mills classical solutions on the twisted torus*, *J. Phys.* **A26** (1993) 2667 [`hep-lat/9206016`].

[7] A. González-Arroyo and Á. Montero, *Self-dual vortex-like configurations in* SU(2) *Yang-Mills theory*, *Phys. Lett.* **B 442** (1998) 273 [`hep-th/9809037`].

[8] Á. Montero, *Study of* SU(3) *vortex-like configurations with a new maximal center gauge fixing method*, *Phys. Lett.* **B 467** (1999) 106 [`hep-lat/9906010`]; SU(3) *vortex-like configurations in the maximal center gauge*, `hep-lat/9907024`.

[9] Á. Montero, *Vortex configurations in the large-N limit*, `hep-lat/0004002`.

[10] M. García Pérez, A. González-Arroyo, Á. Montero and C. Pena, *Yang-Mills classical solutions and fermionic zero modes from lattice calculations*, *Nucl. Phys.* **63** *(Proc. Suppl.)* (1998) 501 [`hep-lat/9709107`].

[11] G. 't Hooft, *A planar diagram theory for strong interactions*, *Nucl. Phys.* **B 72** (1974) 461;
E. Witten, *Instantons, the quark model and the $1/N$ expansion*, *Nucl. Phys.* **B 149** (1979) 285.

[12] G. 't Hooft, *On the phase transition towards permanent quark confinement*, *Nucl. Phys.* **B 138** (1978) 1;
J.M. Cornwall, *Quark confinement and vortices in massive gauge invariant QCD*, *Nucl. Phys.* **B 157** (1979) 392;
G. Mack, *Properties of lattice gauge theory models at low temperatures*, in *Recent developments in gauge theories*, G. 't Hooft et al. eds., Plenum, New York 1980;
H.B. Nielsen and P. Olesen, *A quantum liquid model for the QCD vacuum: gauge and rotational invariance of domained and quantized homogeneous color fields*, *Nucl. Phys.*

B 160 (1979) 380;
J. Ambjørn and P. Olesen, *On the formation of a random color magnetic quantum liquid in QCD*, *Nucl. Phys.* **B 170** (1980) 60; *A color magnetic vortex condensate in QCD*, *Nucl. Phys.* **B 170** (1980) 265.

[13] L. Del Debbio, M. Faber, J. Greensite and S. Olejnik, *Center dominance and Z_2 vortices in* SU(2) *lattice gauge theory*, *Phys. Rev.* **D 55** (1997) 2298 [hep-lat/9610005];
M. Faber, J. Greensite and S. Olejník, *Casimir scaling from center vortices: towards an understanding of the adjoint string tension*, *Phys. Rev.* **D 57** (1998) 2603 [hep-lat/9710039]; *Center projection with and without gauge fixing*, *J. High Energy Phys.* **01** (1999) 008 [hep-lat/9810008]; *First evidence for center dominance in* SU(3) *lattice gauge theory*, *Phys. Lett.* **B 474** (2000) 177 [hep-lat/9911006];
L. Del Debbio, M. Faber, J. Giedt, J. Greensite and S. Olejník, *Detection of center vortices in the lattice Yang-Mills vacuum*, *Phys. Rev.* **D 58** (1998) 094501 [hep-lat/9801027];
R. Bertle, M. Faber, J. Greensite and S. Olejník, *The structure of projected center vortices in lattice gauge theory*, *J. High Energy Phys.* **03** (1999) 019 [hep-lat/9903023];
M. Faber, J. Greensite, S. Olejník and D. Yamada, *The vortex-finding property of maximal center (and other) gauges*, *J. High Energy Phys.* **12** (1999) 012 [hep-lat/9910033].

[14] K. Langfeld, H. Reinhardt and O. Tennert, *Confinement and scaling of the vortex vacuum of* SU(2) *lattice gauge theory*, *Phys. Lett.* **B 419** (1998) 317 [hep-lat/9710068];
M. Engelhardt, K. Langfeld, H. Reinhardt and O. Tennert, *Interaction of confining vortices in* SU(2) *lattice gauge theory*, *Phys. Lett.* **B 431** (1998) 141 [hep-lat/9801030]; *Center vortices of Yang-Mills theory at finite temperatures*, *Phys. Lett.* **B 452** (1999) 301 [hep-lat/9805002]; *Deconfinement in* SU(2) *Yang-Mills theory as a center vortex percolation transition*, *Phys. Rev.* **D 61** (2000) 054504 [hep-lat/9904004];
M. Engelhardt and H. Reinhardt, *Center projection vortices in continuum Yang-Mills theory*, *Nucl. Phys.* **B 567** (2000) 249 [hep-th/9907139]; *Center vortex model for the infrared sector of Yang-Mills theory: confinement and deconfinement*, hep-lat/9912003.

[15] B.L.G. Bakker, A.I. Veselov and M.A. Zubkov, *Central dominance and the confinement mechanism in gluodynamics*, *Phys. Lett.* **B 471** (1999) 214 [hep-lat/9902010].

[16] P. de Forcrand and M. D'Elia, *On the relevance of center vortices to QCD*, *Phys. Rev. Lett.* **82** (1999) 4582 [hep-lat/9901020];
C. Alexandrou, M. D'Elia and P. de Forcrand, *The relevance of center vortices*, hep-lat/9907028.

[17] T.G. Kovács and E.T. Tomboulis, *Vortices and confinement at weak coupling*, *Phys. Rev.* **D 57** (1998) 4054 [hep-lat/9711009]; *Absence of confinement in the absence of vortices*, *J. Math. Phys.* **40** (1999) 4677 [hep-lat/9806030]; *Vortices and the* SU(3)

string tension, *Phys. Lett.* **B 443** (1998) 239 [hep-lat/9807027]; *On p-vortices and the gribov problem*, *Phys. Lett.* **B 463** (1999) 104 [hep-lat/9905029]; *Computation of the vortex free energy in* SU(2) *gauge theory*, hep-lat/0002004.

[18] A. González-Arroyo and P. Martínez, *Investigating Yang-Mills theory and confinement as a function of the spatial volume*, *Nucl. Phys.* **B 459** (1996) 337 [hep-lat/9507001].

[19] A. González-Arroyo, P. Martínez and A. Montero, *Gauge invariant structures and confinement*, *Phys. Lett.* **B 359** (1995) 159 [hep-lat/9507006];
A. González-Arroyo and A. Montero, *Do classical configurations produce confinement?*, *Phys. Lett.* **B 387** (1996) 823 [hep-th/9604017].

[20] K.G. Wilson, *Confinement of quarks*, *Phys. Rev.* **D 10** (1974) 2445.

[21] N. Cabibbo and E. Marinari, *A new method for updating* SU(N) *matrices in computer simulations of gauge theories*, *Phys. Lett.* **B 119** (1982) 387;
M. Okawa, *Monte Carlo study of the Eguchi-Kawai model*, *Phys. Rev. Lett.* **49** (1982) 353.

[22] Á. Montero, *Confinamiento y configuraciones clásicas*, Ph. D. thesis Universidad Autónoma de Madrid 1998.

JHEP05(2000)022